lengths than would be accessible with the usual crystal monochromator (Section 2.3.4.1.2). The idea of supermirrors, comprising bilayers of graduated thickness, and in effect increasing the critical angle, was suggested by Turchin (1967) and Mezei (1976). For a perhaps simplistic explanation, we note first that since the bilayer dimension d is large compared with the neutron wavelength, we can approximate the above equation for reflection as

$$\theta \simeq \lambda \frac{1}{2d},$$

in which form it is reminiscent of equation (2.3.6). If we take $d_{\min}$ to be the thickness of the thinnest bilayer, then we can propose that the critical angle for reflection by the supermirror should be

$$\theta_c^{\rm SM} \simeq \lambda \frac{1}{2d_{\min}}. \qquad (2.3.13)$$

In order to ensure that all neutrons incident at angles less than this critical angle should be reflected, we need to incorporate a more-or-less continuous range of thicker bilayers into the supermirror (Fig. 2.3.14*b*). A more rigorous treatment (Hayter & Mook, 1989; Masalovich, 2013) takes account of the transmission and reflection at each interface, and lays down a prescription as to how the thicknesses should be varied. The most common pairing for the bilayer is now Ni with Ti; the coherent scattering cross sections are of opposite sign (see Table 2.3.2). The performance of a supermirror is normally quoted as the ratio m of the critical angle for the supermirror, $\theta_c^{\rm SM}$, to that for natural nickel, $\theta_c^{\rm Ni}$; a high value for reflectivity is also important. Supermirrors to m of 2 or 3 are in quite common use, while now Ni/Ti supermirrors with m up to 7 are offered for purchase (Swiss Neutronics AG; see also Maruyama *et al.*, 2007).

Consideration is currently being given to the variation of the cross section of the guide along its length. There is some loss on reflection by supermirrors, so these studies aim to reduce the number of reflections involved in transmission along the guide. One suggestion (also attributable to Mezei, 1997) is to use a 'ballistic guide', in which neutrons from the source travel through a taper of widening cross section into a length of larger guide, then through a taper of narrowing cross section to restore the original cross section at the exit. This is said to reduce the number of reflections suffered by the neutron by a factor of $(w_0/w)^2$, where w_0 is the width at entrance and exit and w the larger width along the main part of the guide (Häse *et al.*, 2002). Such a guide has been installed and is operating successfully on the vertical cold source at the Institut Laue–Langevin (Abele *et al.*, 2006). An extension of this idea is based on the well known property of ellipses that a ray emanating from one focus is reflected (just one bounce) to pass through the other; so if the guide cross section could be varied to give a very long ellipse, a source of neutrons placed at one focus, and the target point at the other, then perhaps the neutrons could be transmitted along the guide with just a single reflection (Schanzer *et al.*, 2004; Rodriguez *et al.*, 2011). Accordingly a number of neutron facilities have installed elliptical guides, and indeed a number of neutron powder diffractometers now are located on elliptical guides; these include diffractometer POWTEX at FRM-II, the high-resolution diffractometers HRPD and WISH at ISIS, and Super-HRPD at JSNS. Computer simulation by Cussen *et al.* (2013), however, questions whether, given the practicalities of finite source sizes and the approximation of elliptical variation by a number of linear segments, the theoretical improvement is fully realized.

2.3.4. Diffractometers

Put simply, the diffracted neutron beams associated with the different d-spacings in the sample under study satisfy Bragg's law,

$$\lambda = 2d \sin(\theta). \qquad (2.3.14)$$

As always, λ is the wavelength of the incident neutrons, and these neutrons are scattered through an angle 2θ.

There are basically two ways of exploiting this relationship. The first is to use a single wavelength for the investigation, in which case diffracted neutrons are observed at different angles 2θ corresponding to different d-spacings in the sample. A neutron powder diffractometer designed to carry out an investigation by this means we choose to call a 'constant wavelength' (CW) diffractometer. The other means is to fix the angle 2θ, illuminate the specimen with a range of wavelengths, and note the different wavelengths that are diffracted. In this case, we determine the wavelengths of the diffracted neutrons *via* their speed $\lambda = h/(mv)$ [equation (2.3.1)], and that in turn is measured by their flight time t over a path of length L, $v = L/t$; this leads to

$$\lambda = \frac{ht}{mL}. \qquad (2.3.15)$$

A diffractometer designed to carry out such an analysis of wavelengths we call a 'time-of-flight (TOF) diffractometer'.

The distinction between these two modes of operation can also be indicated *via* the Ewald construction in reciprocal space (Section 1.1.2.4). In this, the ideal powder is represented by concentric spheres in reciprocal space. In the constant-wavelength situation, the primary beam is fixed in direction and the Ewald sphere has a fixed radius; diffracted (reflected) beams are observed at any angle at which the surface of the Ewald sphere intersects one of the concentric spheres mentioned just above. In the wavelength-analysis (time-of-flight) situation, the directions of the primary and diffracted beams are fixed, but the radius of the Ewald sphere ($1/\lambda$) is variable through a range; diffracted beams are observed whenever the wavelength is such that the tip of the vector representing the reflected beam lies on one of the concentric spheres.

2.3.4.1. *Constant-wavelength neutron diffractometers*

The salient features of a constant-wavelength diffractometer are perhaps most easily explained by reference to a particular example; for this purpose we consider the High Resolution Powder diffractometer for Thermal neutrons (HRPT) installed at the SINQ continuous spallation source (Fischer *et al.*, 2000). Neutrons from the source travel through a guide tube to the crystal monochromator, which directs neutrons of a selected wavelength toward the sample. The diffracted neutrons are registered in a detector or detectors that cover a range of angles of scattering from the sample. Collimation is used to better define the directions of the neutron beams; in this instance a primary collimator is included in the guide tube and additional collimation is included between the sample and the position-sensitive detector. The various components will be described in more detail below.

2.3.4.1.1. *Collimation*

There need to be restrictions on the angular divergences of the neutron beams. The divergence of the beam impinging upon the crystal monochromator must be limited to better define the wavelength of the neutrons directed to the sample, whereas the divergences of the beams incident upon and diffracted from

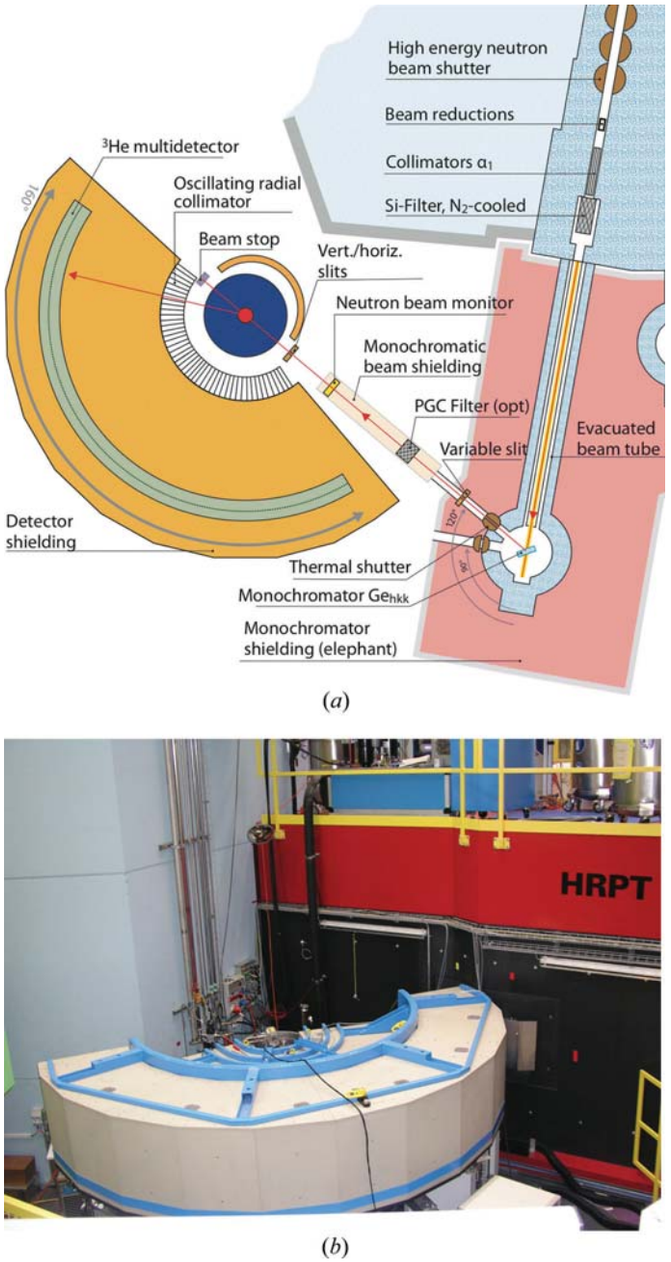

Figure 2.3.15
A constant-wavelength neutron powder diffractometer. This figure shows (*a*) a layout diagram and (*b*) the physical appearance (dominated by the monochromator and detector shieldings) for the HRPT diffractometer installed at the SINQ continuous spallation source. (Figures from https://www.psi.ch/sinq/hrpt/.)

the sample will control the precision with which the scattering angle 2θ can be determined. For a diffractometer detecting neutrons and measuring scattering angles in the horizontal plane (as shown in Fig. 2.3.15) the horizontal divergences are critical, the vertical divergences less so.[11] Indeed, the horizontal divergences are key parameters in the determination of resolution and intensity (Section 2.3.4.1.4); for this reason we denote by α_1, α_2 and α_3 the (half-angle) angular divergences of the primary beam (*i.e.* the beam onto the monochromator), the monochromatic beam (from monochromator to sample) and the diffracted beam (from sample to detector), respectively.

[11] For this reason large vertical divergences are employed to increase intensity; they do however have second-order impacts on the shapes (asymmetry) and positions of diffraction peaks (Howard, 1982; Finger *et al.*, 1994; see also Section 4.2 in Kisi & Howard, 2008).

The divergences are limited by various forms of collimation. The divergence of the primary beam will be limited in the first instance by the delivery system. For delivery through a simple beam tube of length L, with entrance and exit apertures of dimensions a_1 and a_2, respectively, the angular divergence (half-angle) is given by (as already noted in Section 2.3.3.4)

$$\alpha_1 = \frac{a_1 + a_2}{2L}. \tag{2.3.16}$$

Neutrons emerging from a guide tube would have divergence equal to the critical angle of the guide, $\alpha_1 = \theta_c$. Soller collimators (see below) can be used if there is a need to further reduce the horizontal divergence of the primary beam. The divergence of the monochromatic beam may be limited by slits, or a beam tube. The divergence of the diffracted beam, α_3, is often defined using another Soller collimator. Sometimes this divergence is limited just by the dimensions of the sample and the detecting elements; equation (2.3.16) gives α_3 if it now references the sample and detector element dimensions and the distance between them. Even in this circumstance (as in HRPT), Soller collimators may be used in front of the detector to reduce scattering from ancillary equipment and other background contributions.

Soller collimators (Soller, 1924) are used to transmit beams of large cross section while limiting (for example) horizontal divergence. They are in effect narrow but tall rectangular collimators stacked side by side; in practice they comprise thin neutron-absorbing blades equally spaced in a mounting box. It should be evident from equation (2.3.16) that if the length of the collimator is L and the separation between the blades is a, then the (half-angle) horizontal divergence is a/L. The transmission function for a Soller collimator is ideally triangular. It is technologically challenging to make compact Soller collimators, since, for a given collimation, a shorter collimator needs a smaller blade spacing. One very successful approach, due to Carlile *et al.* (1977), has been to make the neutron-absorbing blades from Mylar, stretched on thin steel or aluminium alloy frames, and subsequently coated with gadolinium oxide paint; these blades are stacked and connected *via* the frames which become the spacers in the final product. The collimators made by Carlile *et al.* were 34 cm long, and the blade spacing was 1 mm, giving a horizontal divergence of 0.17°. Compact Soller collimators of this type (Fig. 2.3.16) are now commercially available, with blade spacings down to 0.5 mm.

Even more compact collimators can be produced by eliminating the gaps in favour of solid layers of neutron-transmitting material; for example, a collimator only 2.75 cm long made by stacking 0.16 mm thick gadolinium-coated silicon wafers gave a divergence of 0.33° (Cussen *et al.*, 2001). Microchannel plates (Wilkins *et al.*, 1989) may offer additional possibilities for collimation and focusing.

2.3.4.1.2. *Monochromators*

The wavelength in a constant-wavelength powder diffractometer is almost invariably selected by a single-crystal monochromator. If the primary beam is incident onto the monochromator in such a way as to make an angle θ_M with a chosen set of planes in the crystal, then the wavelength that will be reflected from these planes is given by Bragg's law,

$$\lambda = 2d \sin(\theta_M),$$

where d is the spacing of the chosen planes. A spread of angles of incidence represented by $\Delta\theta_M$ will result in the selection of a

Figure 2.3.16
Commercially available compact Soller collimators. (Reproduced with permission from Eurocollimators Ltd, UK.)

band of wavelengths $\Delta\lambda$ given by

$$\frac{\Delta\lambda}{\lambda} = \cot\theta_M \Delta\theta_M. \qquad (2.3.17)$$

For high-resolution performance we need a rather precisely defined wavelength, so $\Delta\lambda$ should be small; if, on the other hand, intensity is an issue then a wider band of wavelengths needs to be accepted. It should be evident from equation (2.3.17) that a high-resolution diffractometer will operate with a take-off angle from the monochromator, $2\theta_M$, as high (*i.e.* as close to 180°) as practicable, and with tight primary collimation α_1.

It might be noticed that the integer n appearing on the right-hand side of equation (1.1.3) has been omitted from our formulation of Bragg's law. If the Miller indices of the chosen planes are hkl, if the spacing of these planes is d_{hkl}, and if we introduce $d_{nh,nk,nl} = d_{hkl}/n$ [*cf.* equation (1.1.23)], then the factor n is effectively restored. This means that, as well as reflecting the selected wavelength through the hkl reflection, the monochromator has the potential to reflect unwanted harmonics λ/n of the desired wavelength through the nh,nk,nl reflections. This problem can be largely overcome using the hkl planes with h, k, l all odd in crystals with the diamond structure, such as silicon and germanium; for this structure the structure factors [equation (2.3.7)] for the $2h,2k,2l$ reflections are zero so that there is no contamination by $\lambda/2$, and at the shorter wavelengths, $\lambda/3$ and so on, there are very few neutrons in the thermal neutron spectrum (Fig. 2.3.5).

Since 'perfect' crystals (of silicon and germanium, for example) have low reflectivity, for monochromator applications imperfect or 'mosaic' crystals are usually preferred. A mosaic crystal can be pictured as comprising small blocks of crystal with slightly differing orientations, the distribution in angle of these blocks being characterized by a full-width at half-maximum angle, β, known as the 'mosaic spread'. In addition to improving the intensity markedly,[12] this 'mosaic spread' will also increase the range of wavelengths obtained. Crystals intended for use as monochromators are very often deliberately deformed to achieve the desired mosaic structure. Further gains in intensity are sought by using vertically focusing monochromators, since the vertical divergence can be increased without serious detriment to the diffraction patterns. Vertically focusing monochromators usually comprise a number of separate monochromator crystals either individually adjustable (Fig. 2.3.17) or in fixed mountings on a bendable plate.

It is not common to find polarized neutrons being used in neutron powder diffractometers. Nevertheless, we think it appropriate to mention here that one means to obtain a polarized neutron beam is to use an appropriate polarizing crystal monochromator.[13] The 111 reflection from the ferromagnetic Heusler alloy Cu_2MnAl is commonly used for this purpose; the nuclear and magnetic structure factors [equations (2.3.7) and (2.3.8)] are of similar magnitude and they add or subtract depending on whether the neutron spin is antiparallel or parallel to the magnetization of the alloy. The beam reflected from such a monochromator can be polarized to better than 99%.

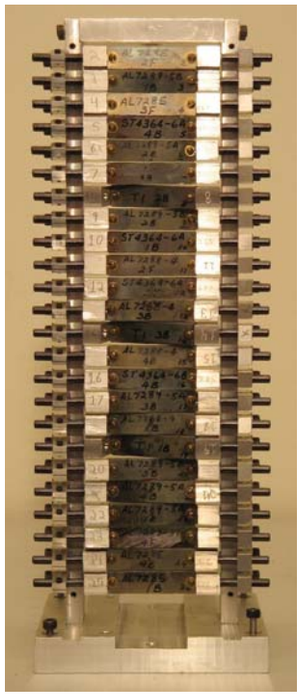

Figure 2.3.17
The vertically focusing monochromator constructed at the Brookhaven National Laboratory (Vogt *et al.*, 1994) and now used by the high-resolution powder diffractometer ECHIDNA at OPAL. The 24 monochromating elements are individually adjustable, and each of these is a 30-high stack of 0.3 mm thick Ge wafers, deformed to yield a suitable mosaic structure and then brazed together. (Reproduced with permission from ANSTO.)

The reader is referred to Section 4.4.2 of Volume C (Anderson & Schärpf, 2006) and to Kisi & Howard (2008) Sections 3.2.1 and 12.3 for further details.

2.3.4.1.3. *Neutron detectors*

Neutrons, being electrically neutral, do not themselves cause ionization and so cannot be detected directly; their detection and counting therefore depend on their capture by specific nuclei and the production of readily detectable ionizing radiation in the ensuing nuclear reaction. Only a limited number of neutron-capture reactions are useful for neutron detection [see Chapter 7.3 of Volume C (Convert & Chieux, 2006)]; they include

$$\begin{aligned}
{}^1_0\mathrm{n} + {}^3_2\mathrm{He} &\rightarrow {}^1_1\mathrm{H} + {}^3_1\mathrm{H} + 0.76\ \mathrm{MeV}\\
{}^1_0\mathrm{n} + {}^6_3\mathrm{Li} &\rightarrow {}^3_1\mathrm{H} + {}^4_2\mathrm{He} + 4.79\ \mathrm{MeV}\\
{}^1_0\mathrm{n} + {}^{10}_5\mathrm{B} &\rightarrow {}^7_3\mathrm{Li} + {}^4_2\mathrm{He} + 2.8\ \mathrm{MeV}\\
{}^1_0\mathrm{n} + {}^{157}_{64}\mathrm{Gd} &\rightarrow {}^{158}_{64}\mathrm{Gd} + \gamma\text{-rays} + \text{conversion electrons}\\
&\quad + \leq 0.18\ \mathrm{MeV}\\
{}^1_0\mathrm{n} + {}^{235}_{92}\mathrm{U} &\rightarrow \text{fission fragments} + \sim 200\,\mathrm{MeV}
\end{aligned}$$

(*cf.* Section 2.3.3.2).

[12] Most of the improvement is due to a change from a 'dynamical' to a 'kinematic' scattering regime.

[13] Polarized beams can also be produced using suitable mirrors or filters [see Section 4.4.2 of Volume C by Anderson & Schärpf (2006)].

The attenuation of neutrons in these materials (Section 2.3.2.4) will be dominated by the high absorption (by capture) cross sections (Table 2.3.2), so the linear attenuation coefficient will be given by $\mu = N\sigma_{\rm abs}$ where N is the number of absorbing nuclei per unit volume. We remark that absorption cross sections, with the exception of Gd, increase linearly with wavelength. The factor by which the neutron beam is diminished in a detector of thickness x is $\exp(-\mu x) = \exp(-N\sigma_{\rm abs}x)$. The detector efficiency, then, given by the fraction of neutrons absorbed (captured) in the detector, is $1 - \exp(-N\sigma_{\rm abs}x)$. In most cases the aim is to have high detector efficiency; however, in some circumstances it is desirable to monitor an incident neutron beam, in which case attenuation should be kept to a minimum. The account of neutron detection given here will be kept relatively brief since much has been written on this subject elsewhere [Oed, 2003; Chapter 7.3 of Volume C (Convert & Chieux, 2006)].

The task, following the neutron-capture reaction, is to detect the various charged particles or ionizing radiations that are produced. These are registered by the electrical signals they generate in a gas-filled proportional counter or ionization chamber, or in a semiconductor detector, recorded on film, or detected from the flashes of light they produce in a scintillator, for example ZnS. It is well worth noting that the secondary radiation carries no record of the energy of the detected neutrons; so whatever the means of detection, detectors can count neutrons but can provide no information on their energy distribution.

The gas-filled radiation detectors are essentially Geiger counters, comprising a gas-filled tube with a fine anode wire running along its centre. The anode collects the electrons released by ionization of the gas; if the anode voltage is high enough, there is a cascade of ionization providing amplification of the signal.[14] Detectors filled with boron trifluoride, $^{10}BF_3$, and helium-3, ^{3}He, have high efficiencies and are in common use; in these the nucleus designated to capture neutrons is incorporated in the filling gas. Such detectors operate with pulse-height discrimination, not in any attempt to determine neutron energy, but to discriminate against lower-voltage signals from γ-rays and other unwanted background. Another approach is to have a thin solid layer[15] of neutron-absorbing material, ^{235}U for example, releasing secondary radiation, in this case fission products, into a gas proportional counter filled with a standard argon/methane mixture; this would represent a low-efficiency neutron detector suitable for use as an incident-beam neutron monitor. Neutron detection based on semiconductor particle detectors is still in the developmental stage. The main problem is that the semiconductors used for charged-particle detection do not contain neutron-absorbing isotopes. Semiconductor particle detectors could be used to register the secondary radiation from an abutting layer of neutron-absorbing solid, but that layer would need to be thin, and another low-efficiency neutron detector would result. Scintillation detectors involve the placement of neutron-absorbing materials, such as ^{6}LiF, adjacent to a scintillator such as a ZnS screen, or perhaps the use of a Ce-doped lithium silicate glass, and counting the flashes of light that are produced. These light flashes can be recorded by photomultiplier tubes or on film. Scintillation detectors are, however, not used in constant-wavelength diffractometers because of their sensitivity to γ-radiation. They are used in time-of-flight diffractometers at spallation sources by exploiting the fact that the unwanted fast neutrons and γ-rays, and the thermal neutrons of interest, are separated in time (Section 2.3.4.2.2).

Much of the preceding description refers to single neutron counters, although it should be noted that there is a position-sensitive capability inherent in a film or scintillator screen. The earliest CW diffractometers employed just a single detector set on an arm that scanned through the scattering angle 2θ; the deployment of a Soller collimator just in front of the detector was advantageous. Conceptually the simplest but not necessarily the cheapest means for improvement was to mount a number of collimator/detector pairs on the detector arms. Such an improvement was made to diffractometer D1A at the Institut Laue–Langevin (Hewat & Bailey, 1976) by mounting ten sets of 10′ divergence Soller collimators/^{3}He detectors at intervals of 6°. The BT-1 diffractometer at NBSR operates with 32 ^{3}He detectors set at 5° intervals, so a scan through 5° covers a total angular range of 160°. The ultimate level for this kind of development was reached when D2B at the Institut Laue–Langevin operated in its former mode, with 64 detectors set at 2.5° intervals, each with its own 5′ Mylar Soller collimator; this required a scan through only 2.5° to record 160° of diffraction.

The alternative to using large numbers of individual detectors is to make use of position-sensitive neutron detectors (PSDs), and these have been in use for quite some time. The technology is that of the position-sensitive detection of charged particles, the important issue for neutrons being that the charged-particle detection should be located close to the neutron-capture event so that positional information is retained. A gas-filled ^{3}He detector with a single anode wire can serve as a linear PSD, for example by comparing the charges collected, after the capture event, at the opposite ends of the wire. The D2B diffractometer at the Institut Laue–Langevin has now been upgraded to 'SuperD2B', which uses 128 linear PSDs with their axes (anode wires) vertical, at 2θ intervals of 1.25°; this operates as a quasi-two-dimensional PSD. Diffractometers SPODI at FRM-II (80 detectors) and ECHIDNA at OPAL (128 detectors) are fitted with similar detector arrays. A single gas-filled chamber containing a number of separate parallel vertically aligned anodes, termed a multi-wire proportional counter (MWPC), provides another approach; the electronics needs to register at which of the wires the capture event occurred. This technology has extended from the first multi-wire PSD with 400 wires at 5 mm (0.2°) separation, used on the D1B diffractometer at the Institut Laue–Langevin in the 1970s, to a PSD with 1600 wires at 0.1° separation now in use on HRPT at SINQ (Fig. 2.3.15). A further advance is the development of the micro-strip gas chamber (MSGC) detector (Oed, 1988). In this detector the anodes and the cathodes are printed circuits on glass substrates, which are then mounted into the chamber. With this arrangement, an anode separation of 1 mm is achievable and the stability is excellent. The high-intensity diffractometer D20 at the Institut Laue–Langevin has a detector assembled from plates of micro-strip detectors and achieves 1600 anodes at 0.1° angle separation.

As pointed out above, the detection systems on SuperD2B, SPODI and ECHIDNA achieve a quasi-two-dimensional position capability by using banks of linear PSDs located side by side. An MWPC detector can achieve two-dimensional capability in a very similar manner, using the anode position to locate in the horizontal direction and charge division measurements at the ends of each anode wire to find the vertical position. An MWPC detector can also be fitted with segmented cathodes, either side of the anodes, one returning positional information in the horizontal

[14] Strictly speaking, the term 'Geiger counter' should be reserved for detectors operating in this amplification regime.
[15] The layer must be thin so that the secondary radiation, which has a short range in solids, can escape into the charged-particle detector.

direction and the other giving the vertical position. A detector of this kind is used on the WOMBAT diffractometer at the OPAL reactor. MSGC detectors can also be adapted to provide two-dimensional positional information after printing a set of cathodes orthogonal to the primary set on the back surface of the glass.

A few general comments about detecting systems are in order. The time for a detector to recover after registering a neutron count is known as the dead time, and this may be significant when count rates are high, in which case corrections are needed [Chapter 7.3 of Volume C (Convert & Chieux, 2006)]. For banks of detectors, and also for position-sensitive detectors, calibration for position and sensitivity becomes a critical issue. In the case of a smaller bank of detectors, it may be possible to scan the detector bank so the same diffraction pattern is recorded in the different detectors, in which case the relative positions and efficiencies of the different detectors can be determined quite well (see Section 4.1 of Kisi & Howard, 2008). For more extensive banks or large position-sensitive detectors, detector sensitivity calibration is performed by examining the very nearly isotropic incoherent scattering from vanadium. In this case checking for angular accuracy can be more difficult. The time taken to register a neutron count cannot be said to be a fundamental issue in CW powder diffraction, since in some applications it is scarcely relevant, although in other applications, such in the study of very fast reaction kinetics (Riley *et al.*, 2002), the constraints on time are very demanding.

2.3.4.1.4. *Resolution and intensity*

The resolution and intensity of a CW powder diffractometer are strongly influenced by the divergences α_1, α_2 and α_3 of the primary, monochromatic and diffracted beams, respectively, along with the mosaic spread β of the crystal monochromator. The situation was analysed by Caglioti *et al.* (1958) on the basis that the triangular transmission factor of each collimator, total width 2α, could be approximated by a Gaussian with full-width at half-maximum (FWHM) α, that the mosaic distribution of the monochromator could also be described by a Gaussian with FWHM β, but that there was no sample contribution to the peak widths. On this basis the diffraction peaks were found to be Gaussian, with the FWHM of the diffraction peak occurring at scattering angle 2θ given by (Hewat, 1975)

$$\mathrm{FWHM}^2 = U\tan^2\theta + V\tan\theta + W, \tag{2.3.18}$$

where

$$U = \frac{4(\alpha_1^2\alpha_2^2 + \alpha_1^2\beta^2 + \alpha_2^2\beta^2)}{\tan^2\theta_M(\alpha_1^2 + \alpha_2^2 + 4\beta^2)}, \tag{2.3.18a}$$

$$V = \frac{-4\alpha_2^2(\alpha_1^2 + 2\beta^2)}{\tan\theta_M(\alpha_1^2 + \alpha_2^2 + 4\beta^2)}, \tag{2.3.18b}$$

$$W = \frac{\alpha_1^2\alpha_2^2 + \alpha_1^2\alpha_3^2 + \alpha_2^2\alpha_3^2 + 4\beta^2(\alpha_2^2 + \alpha_3^2)}{\alpha_1^2 + \alpha_2^2 + 4\beta^2} \tag{2.3.18c}$$

and θ_M is the Bragg angle ($2\theta_M$ is the take-off angle) at the monochromator. Under these conditions the total (integrated) intensity in the diffraction peak is given by

$$L \propto \frac{\alpha_1\alpha_2\alpha_3\beta}{(\alpha_1^2 + \alpha_2^2 + 4\beta^2)^{1/2}}. \tag{2.3.19}$$

These equations have important implications and accordingly have received a good deal of attention. They return at once the well known resolution advantage in setting up the diffractometer in the parallel configuration (that seen in Fig. 2.3.15, in this configuration θ_M taken to be positive). Caglioti *et al.* (1958) deduced that for the simple case of $\alpha_1 = \alpha_2 = \alpha_3 = \beta = \alpha$ equations (2.3.18) and (2.3.19) reduce to

$$\mathrm{FWHM} = \alpha\left(\frac{11 - 12a + 12a^2}{6}\right)^{1/2} \text{ and } L \propto \alpha^3/(6)^{1/2},$$

where $a = \tan\theta/\tan\theta_M$; they went on to record results for a number of other combinations. In his design for a high-resolution diffractometer, Hewat (1975) considered the case $\alpha_2 = 2\beta > \alpha_1 \simeq \alpha_3$. Under these conditions, the peak widths are close to their minimum around the parallel focusing condition $\theta = \theta_M$, their widths there are given by

$$\mathrm{FWHM}^2 = (\alpha_1^2 + \alpha_3^2) - \frac{\alpha_1^4}{\alpha_1^2 + \alpha_2^2 + 4\beta^2} \simeq \alpha_1^2 + \alpha_3^2,$$

and the total intensity is approximately

$$L \propto \alpha_1\alpha_3\beta/(2)^{1/2}.$$

Hewat's conclusions, put briefly, were that good resolution could be obtained by keeping divergences α_1 and α_3 small, while intensity could be somewhat recovered by adopting relatively large values for the monochromator mosaic spread β and divergence α_2 of the monochromatic beam. Hewat also argued for a high monochromator take-off angle $2\theta_M$, not only to reduce peak widths [through the term $\cot\theta_M$ appearing in equation (2.3.17) and reappearing in equations (2.3.18)], but also to match the region of best resolution to that of the most closely spaced peaks in the diffraction pattern. Hewat's design was implemented in the D1A diffractometer at the Institut Laue–Langevin (Hewat & Bailey, 1976), subsequently in the D2B diffractometer at the same establishment, and elsewhere. In a version installed at the (now retired) HIFAR reactor in Sydney, Howard *et al.* (1983), using an Al_2O_3 (corundum) ceramic sample, reported a peak-width variation in close agreement with that calculated from equation (2.3.18). Although more sophisticated analyses are available in the literature (Cussen, 2000), this result would suggest that equations (2.3.18) still provide a good starting point.

The usual trade-off between intensity and resolution applies, and since neutron sources are rather less intense than X-ray sources, this is an important consideration. Intensity is sacrificed by using high monochromator take-off angles to limit the wavelength spread [equation (2.3.17)], and by using tight collimation [equation (2.3.19)]. Evidently intensities could be increased by relaxing these constraints. These days it is more common to build diffractometers of good-to-high resolution, and then to seek other means to improve data-collection rates. Focusing monochromators, such as described in Section 2.3.4.1.2, serve to increase the neutron intensity at the sample position without seriously degrading the resolution. In addition, the use of multi-detector banks and the development and deployment of position-sensitive detectors, as described in Section 2.3.4.1.3, has been very much driven by the desire to increase the speed of data collection. As mentioned earlier, the design and analysis of neutron powder diffractometers should be treated in a holistic fashion, and although some advanced analytical methods have been applied (Cussen, 2016 and references therein), Monte Carlo analyses using programs such as *McStas* (Willendrup *et al.*, 2014) and *VITESS* (Zendler *et al.*, 2014) to track large numbers of neutrons from the source right through to the neutron detectors are now widely employed.

references